ACS APPLIED MATERIALS & INTERFACES

Research Article

Cite This: ACS Appl. Mater. Interfaces 2019, 11, 15447−15456

www.acsami.org

Novel Cellulose−Halloysite Hemostatic Nanocomposite Fibers with a Dramatic Reduction in Human Plasma Coagulation Time

Ranodhi N. Udangawa,[†,‡] Paiyz Esmat Mikael,[‡] Chiara Mancinelli,[†] Caitlyn Chapman,[†] Charles F. Willard,[§] Trevor John Simmons,[∥] and Robert J. Linhardt*[,†,‡,§,∥]

[†]Department of Chemistry and Chemical Biology, [‡]Center for Biotechnology and Interdisciplinary Studies, [§]Department of Chemical and Biological Engineering, and [∥]Rensselaer Nanotechnology Center, Rensselaer Polytechnic Institute, Troy, New York 12180-3590, United States

Supporting Information

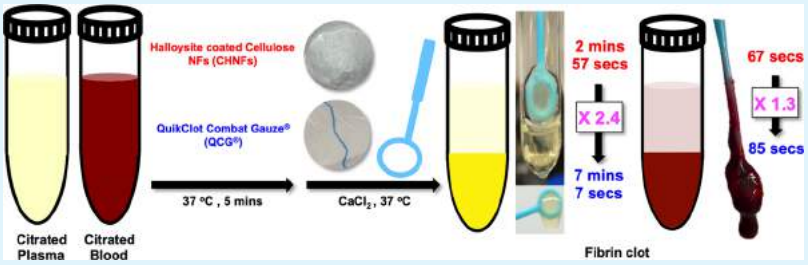

ABSTRACT: High-performance cellulose−halloysite hemostatic nanocomposite fibers (CHNFs) are fabricated using a one-step wet−wet electrospinning process and evaluated for human plasma coagulation by activated partial thromboplastin time. These novel biocompatible CHNFs exhibit 2.4 times faster plasma coagulation time compared with the industry gold standard QuikClot Combat Gauze (QCG). The CHNFs have superior antileaching property of clay with 3 times higher post-wetting clotting activity compared to QCG. The CHNFs also coagulate whole blood 1.3 times faster than the QCG and retain twice the clotting performance after washing. Halloysite clay is also more effective in plasma coagulation than commercial kaolin clay. The physical and thermal properties of the CHNFs were evaluated using scanning electron microscopy, energy-dispersive X-ray spectroscopy, X-ray diffraction, Brunauer−Emmett−Teller surface area analysis, and thermogravimetric analysis. CHNFs show a 7-fold greater clay loading than QCG and their small average diameter of 450 ± 260 nm affords a greater specific surface area (33.6 $m^2 g^{-1}$) compared with the larger average diameter of 12.6 ± 0.9 μm for QCG with a specific surface area of 1.6 $m^2 g^{-1}$. The CHNFs were shown to be noncytotoxic and human primary fibroblasts proliferated on the composite material. The drastic reduction in coagulation time makes this novel nanocomposite a potential lifesaving material for victims of rapid blood loss such as military personnel and patients undergoing major surgical procedures or to aid in the treatment of unexpected bleeding episodes of patients suffering from hereditary blood clotting disorders. Since a person can die within minutes of heavy bleeding, every second counts for stopping traumatic hemorrhaging.

KEYWORDS: *hemostatic, cellulose, halloysite clay, kaolin clay, electrospinning*

INTRODUCTION

There remains an urgent need in the medical community for the development of novel hemostatic agents to treat hemorrhage associated with traumatic injuries, surgical procedures, and frequent bleeding events resulting from blood coagulation disorders.[1] Patients suffering from hereditary blood clotting disorders, such as hemophilia and von Willebrand disease, suffer from often unexplained and recurrent internal and external bleeding episodes throughout their lives. These external bleeding episodes include prolonged nosebleeds (epistaxis), bleeding from the gums, and excessive bleeding from small cuts or wounds. Even though many of these episodes are non-life-threatening, they can cause extreme discomfort in such patients. In the case of severe hemorrhage, it is critical to cease bleeding as quickly as possible to prevent imminent death. In a battlefield, most fatalities are due to severe hemorrhage and transpire within the first hour of receiving a wound. Thus, the patient's chance of survival depends on the ability of a first responder to minimize blood loss.

There have been a number of topical antihemorrhagic agents designed and developed to stop external hemorrhages. Many consist of a polymer or polymer blend mixed with a blood-clotting agent. HemCon, Chitoseal, Celox, Celox-D, and WoundStat represent several commercially available wound dressings that contain the biopolymer chitosan as the hemostatic agent.[2,3] Most common commercially available hemostatic dressings are produced either by immersing or

Received: March 14, 2019
Accepted: April 12, 2019
Published: April 12, 2019

DOI: 10.1021/acsami.9b04615
ACS Appl. Mater. Interfaces 2019, 11, 15447−15456

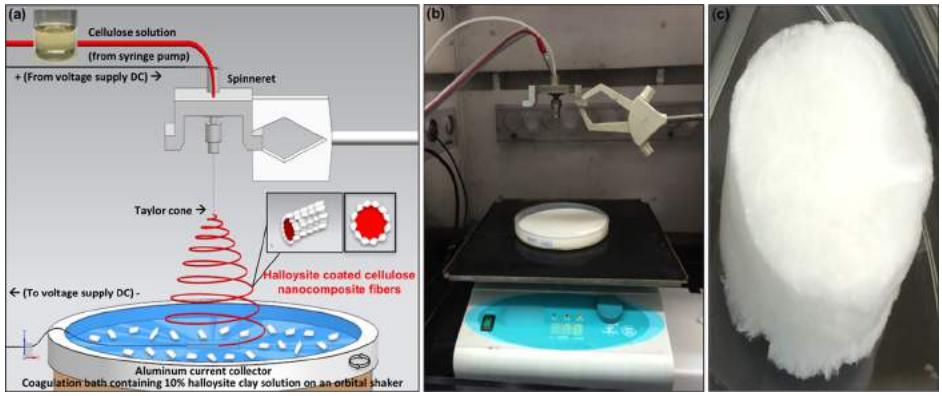

Figure 1. Wet−wet, monoaxial electrospinning process and the method for preparing halloysite clay-coated CNFs. (a) Schematic of the process, (b) photograph of the process, and (c) photograph of halloysite-coated cellulose nanocomposite fibers (CHNFs) after collection and freeze-drying.

spraying the fibrous substrate with a slurry or suspension containing a clotting agent.[4−7] A new sterile gauze pad developed recently using bentonite and halloysite clay has shown to decrease the blood-clotting time in Wistar albino rats. This material was developed by curing a mixture of bentonite and halloysite clay in petroleum jelly onto gauze pads.[7] These products fail to provide prolonged clotting activity because of the loss of clotting agent due to leaching. Extrusion of blends of polymers and clotting agents has also been used to produce hemostatic fibrous materials.[8] However, the clotting agents inside these fibers have minimum or no contact with the external environment, making these ineffective in promoting coagulation. Furthermore, the heterogeneous nature of extrusion processes can negatively impact the mechanical properties of these polymeric fiber products.

Naturally occurring aluminosilicate clay is the most popular choice of hemostatic agent used in a wide range of hemostatic wound dressings.[9] Kaolin aluminosilicate clay promotes coagulation by activating factor XII (Hageman factor) of the coagulation cascade without an accompanying exothermic reaction.[7,10] In contrast, zeolite clays release thermal energy upon contact with the water in the blood, and this exothermic reaction can cause second-degree burns in patients treated with zeolite-based hemostatic products. Thus, the current generation of clay-based topical hemostatic wound dressings almost exclusively contains kaolin clay.[4]

Halloysite ($Al_2Si_2O_5(OH)_4{\cdot}2H_2O$) is a naturally occurring aluminosilicate nanoclay that exhibits a unique hollow tubular scroll structure.[11,12] It has been demonstrated to be biocompatible[13,14] and to promote blood coagulation.[11,15] Halloysite nanotubes are less toxic than sodium chloride table salt and easily removed from an organism by macrophages. Several studies show that halloysite nanotubes are safe to be used as oral drug delivery systems, creams, implants, and wound treatment materials.[13] In studies performed on rabbit blood, hemolysis ratios less than 0.5% were observed, indicating the nonhemolytic nature of the halloysite nanotubes.[15] In recent years, halloysite clay has sparked the interest of the scientific community working on biomaterials and has inspired a number of studies exploring its various applications. Some of these include its use in antimicrobial materials, as drug delivery scaffolds, and in cosmetic applications.[11,12,16,17] Cellulose is often chosen as a matrix on which the nanoclay can be immobilized because of its biocompatibility, low cost, and extensive use in wound dressings.[18,19] Electrospinning has been widely used for preparing synthetic micro- and nanopolymeric fibers from solutions of polymers in volatile organic solvents.[20−23] However, biopolymer cellulose is a complex polysaccharide that does not dissolve in volatile organic solvents because of its extensive hydrogen-bonding network.[24] A special class of nonvolatile solvents, known as room-temperature ionic liquids (RTILs), is required for electrospinning of cellulose.[25−28] The electrospinning of cellulose from a nonvolatile RTIL, referred to as wet−wet electrospinning, is quite different from the conventional wet−dry electrospinning of a synthetic polymer from a volatile organic solvent.[26,29] In wet−wet electrospinning, a biopolymer, such as cellulose, is dissolved in a nonvolatile primary solvent, typically an RTIL, which is miscible with the secondary solvent, such as water or alcohol, in the coagulation bath collector. This secondary solvent selected for use in the coagulation bath needs to be a nonsolvent of the polymer to promote its precipitation in the coagulation bath.[30] In the case of cellulose electrospinning, RTILs are the most commonly used primary solvent and water or water−ethanol mixtures are the general secondary (or coagulation) solvent.[28,31]

In the current study, halloysite nanoclay was physically embedded onto the cellulose nanofibers (CNFs) by suspending halloysite nanoclay in the coagulation bath secondary solvent. This one-step process affords halloysite-coated cellulose nanofibers (CHNFs). The resulting CHNFs are thoroughly washed with alcohol−water mixture to remove the residual RTIL.[32] QuikClot Combat Gauze (QCG), marketed by Z-MEDICA, LLC,[5,33,34] approved by the United States Food and Drug Administration (FDA), and also endorsed by the US Department of Defense for external use because of its ability of controlling severe arterial hemorrhage,[10,35,36] was selected as the commercial standard to compare the procoagulant efficacy of these CHNFs. As the CHNFs are intended for use as an emergency clotting gauze and not as a wound dressing, this precludes studies such as fluid uptake, water vapor transmission, and antimicrobial activity, which are irrelevant in this situation because of the very short time scale of application (on the order of minutes). These studies would be important in the design of wound dressings, which are intended for long-term use on the order of several hours or days.[37] The CHNFs are envisioned to be stacked, filled into, and supported by a gauze pad, such as typical medical cotton wool-filled wound dressing pads. These gauze pads are made out of a thin layer of highly porous material, which would allow for intimate contact between the blood and the CHNFs.

DOI: 10.1021/acsami.9b04615
ACS Appl. Mater. Interfaces 2019, 11, 15447−15456

EXPERIMENTAL SECTION

Materials. Pure absorbent cotton balls (CVS health sterile cotton balls) were purchased from a local pharmacy. HPLC-grade RTIL, 1-ethyl-3-methylimidazolium acetate ([EMIM][Ac], ≥95.0%), absolute ethanol (≥99.8%), and halloysite nanoclay, a product of Applied Minerals Inc., were obtained from Sigma-Aldrich (St. Louis, Missouri, USA). Kaolin clay was also purchased from Sigma-Aldrich that meets the USP testing specifications. QCG developed by Z-Medica LLC (New York, New York, USA) was obtained from a popular online seller. Citrated human plasma, Pacific Hemostasis activated partial thromboplastin time (aPTT) clinical diagnostic kit, Dulbecco's modified Eagle's medium (DMEM/F12), 10% fetal bovine serum (FBS), and Alamar Blue cell viability reagent were acquired from Thermo Fisher Scientific LLC (Waltham, MA, USA). Citrated bovine whole blood (3.2% sodium citrate) was obtained from BioIVT (Hicksville, NY, USA) and human primary fibroblasts (hFB) were obtained from Lonza (Basel, Switzerland). Paraformaldehyde in phosphate-buffered saline (4% solution ChemCruz) was purchased from Santa Cruz Biotechnology Inc. (Dallas, Texas, USA). Double-distilled water from an in-house water purification system was used for all the relevant experiments mentioned in this study.

Preparation of Fibers. Cotton balls (1.06 g) were mixed with 50.0 g of RTIL ([EMIM][Ac] density = 1.027 g/mL) using a magnetic stirrer at 80 °C for 12 h to obtain a 2.12% (w/w) homogeneous cellulose solution. A halloysite nanoclay suspension (10% (w/v)) was prepared by mixing 10 g of halloysite nanoclay in 100 mL of distilled water. The clay solution was then transferred into a large glass Petri dish and placed on top of an orbital shaker. A schematic and a photograph of the wet−wet, monoaxial electrospinning process are shown in Figure 1a,b. A small piece of aluminum foil was placed inside the Petri dish and connected to the negative lead of a high-voltage supply (CZE1000R, Spellman, Hauppauge, New York, USA) using electrically insulated copper wires. This high-voltage electrospinning system is capable of generating a dc voltage up to 30 kV. The electrospinning process used in this study is based on previously published work on electrospinning of cellulose fibers.[31,38−44] The electrospinning parameters (i.e., needle diameter, distance between electrodes, polymer concentration, flow rate, etc.) were optimized by an interactive approach similar to that of any novel electrospinning study.[31,45]

The cellulose solution was placed in a Norm-Ject syringe (10 mL) that was connected to a spinneret (MECC, Ogori, Fukuoka, Japan) with a fitted aluminum needle. The needle used has a blunt tip with an internal diameter of 0.635 mm (23 gauge). Polytetrafluoroethylene tubing is used to deliver the cellulose solution from the syringe to the spinneret. The spinneret was connected to the positive terminal of the high-voltage supply. The distance between the tip of the aluminum needle and the surface of the clay solution was fixed at 10 cm. Finally, a high voltage of 18 kV was applied between the spinneret set up and the coagulation bath as the cellulose solution was pumped at a constant rate of 60 μL/min into the clay suspension (coagulation bath) using a NE-1000 mechanical syringe pump from New Era Pump Systems Inc. (Wantagh, New York, USA). The orbital shaker was run at 70 rpm to prevent sedimentation of clay on the bottom of the Petri dish. At the end of the spinning process, the solidified cellulose-halloysite fibers were removed from the coagulation bath and transferred into a clean 50% distilled water−ethanol bath to further remove ionic liquid from the fibers.[46] Finally, the fibers were freeze-dried to obtain the halloysite clay-coated CNFs, CHNFs (Figure 1c).

This electrospinning process was repeated using a distilled water coagulation bath instead of the halloysite nanoclay suspension, to produce CNFs as a negative control. CNFs after electrospinning were mixed with halloysite clay (halloysite clay mixed cellulose nanofibers, MCHNFs) and were used as a second control to evaluate the commonly used method of fiber production in the commercial products previously described. This process for producing MCHNFs involves immersing electrospun CNFs in a halloysite nanoclay suspension (10% (w/v)) for 24 h. The MCHNFs were then transferred into a clean 50% distilled water−ethanol bath for a washing step. Finally, the fibers were freeze-dried to obtain the halloysite clay-mixed CNFs, MCHNFs. All of the electrospinning processes were carried out inside an antistatic polycarbonate box within a standard laboratory fume hood at 20 ± 3 °C with a relative humidity controlled at 59 ± 5%. AcuRite digital humidity and temperature monitor was used to measure the temperature and the relative humidity. When referring to washed CHNFs and QCG composites, the samples were additionally vigorously stirred in a beaker of distilled water for 1 min.

Characterization. *Thermogravimetric Analysis.* CHNFs, MCHNFs, CNFs, and QCG were subjected to thermogravimetric analysis (TGA-Q50 apparatus, New Castle, Delaware, USA) to deduce the amount of clay present in the fiber composites. The composite fibers before and after a water wash were also analyzed along with halloysite and kaolin clay controls. All the samples were heated from room temperature (25 °C) to 1000 °C at a constant heating rate of 10 °C/min under dry atmospheric conditions. The average decomposition temperatures and the final ash contents were determined by TA Instruments Universal Analysis software V4.7A. Furthermore, TA Instruments define the detection limit of TGA as 0.1% by mass of the sample.[47]

Morphology and Elemental Composition. A Carl Zeiss Supra field emission scanning electron microscope (Hillsboro, USA—resolution at 1 kV—2.5 nm) with energy-dispersive X-ray (EDX) spectroscopy was used to investigate the morphology and the elemental composition of the CHNFs. QCG was imaged before and after subjecting to a washing step to empirically evaluate the leaching of kaolin clay from the fibers. CNFs, halloysite nanoclay, and kaolin clay were also subjected to SEM and EDX analysis as controls. The average fiber diameters were calculated using NIH ImageJ software (National Institute of Health, MD, USA). Diameters from 100 individual fibers from 10 identical electrospinning experiments were employed in this fiber diameter analysis.

Crystalline Structure. Crystallinity of the clay in the CHNFs and QCG was studied using a Bruker D8-DISCOVER X-ray diffractometer and compared to halloysite and kaolin clay controls. The crystallinity of the CNFs was also evaluated. The X-ray diffraction (XRD) pattern analysis was performed using Bruker's DIFFRAC.EVA software.

Specific Surface Area. The surface area of the CHNFs was estimated by conducting a Brunauer−Emmett−Teller (BET) surface area analysis using a Quantachrome Autosorb IQ system (Boynton Beach, Florida, USA). A sample of CHNFs (117 mg) was degassed at 100 °C for 24 h. This was followed by N_2 adsorption−desorption at 77.35 K (−196 °C) under a relative vapor pressure (P/P_0) of 0.05−0.3.[48] An electrospun CNF sample (70 mg) was used as a control in this experiment. QCG samples before (447 mg) and after (241 mg) undergoing a washing step were also subjected to surface area analysis using the same experimental conditions as CHNFs. Quantachrome ASiQwin V 4.01 software was used to analyze the adsorption−desorption data and construct the BET/Langmüir plots.

Plasma Clotting Assay. aPTT assay was employed to evaluate the coagulation performance of the CHNFs, QCG, clay controls, and CNFs using citrated human plasma. This assay is a two-step process that measures the time taken to form a fibrin clot in a citrated plasma sample. A sample of citrated human plasma (1 mL) was incubated with ∼1 mg of fiber or clay sample (the activator) for 5 min followed by the addition of 500 μL of 25 mM Pacific Hemostasis calcium chloride solution at 37 °C. A stopwatch was turned on immediately upon the introduction of calcium chloride solution. An inoculating loop was used to detect the formation of the fibrin clot and the time taken to form the fibrin clot was recorded. The inoculating loop is passed through the submerged reaction tube until the fibrin clot is retracted with the loop. Similar procedures have been reported in the literature.[49,50] Because of the unique feature of having a solid composite hemostatic clotting material in the tube, experience showed that the reliability of clot detection was improved over the conventional tilt method[51−53] by using this inoculating loop method. This process was repeated with CHNFs and QCG before and after

DOI: 10.1021/acsami.9b04615
ACS Appl. Mater. Interfaces 2019, 11, 15447−15456

subjecting to a washing step to evaluate the depletion of coagulation performance because of the loss of clay from the composite fibers. A positive control experiment was conducted using 200 μL of citrated human plasma, 100 μL of calcium chloride, and 100 μL of the particle-based Kontact activator (which contains 1.2% rabbit brain phospholipid, 0.03% magnesium aluminum silica, 0.4% phenol, 0.8% buffer, salt, and stabilizers) of the standard Pacific Hemostasis aPTT assay. All the above clotting experiments were run in borosilicate glass culture tubes.

Blood Clotting Test. The blood coagulation activity of the CHNFs and QCG was evaluated using citrated bovine whole blood. A sample of citrated bovine whole blood (1 mL) was incubated with ~1 mg of the fiber sample for 5 min followed by the addition of 500 μL of 25 mM calcium chloride solution at 37 °C. A stopwatch was turned on immediately upon the introduction of calcium chloride solution. An inoculating loop was used to detect the formation of the fibrin clot and the time taken to form the fibrin clot was recorded. This process was repeated with CHNFs and QCG before and after subjecting to a washing step to evaluate the depletion of coagulation performance because of the loss of clay from the composite fibers. All the above clotting experiments were run in borosilicate glass culture tubes.

Biocompatibility Assessment—Cytotoxicity and Cell Viability. hFB were grown in DMEM/F12 supplemented with 10% FBS at 37 °C and 5% CO_2. Prior to cell seeding, the electrospun fiber samples and QCG samples were sterilized in 70% ethanol for 10 min, followed by 10 min of UV exposure. hFB cells were seeded at 150 000 cells/cm^2. The cells were allowed to adhere for 1 h before the addition of 1 mL of fresh media. Alamar Blue cell metabolic activity assay was used according to the instructions of the manufacturer to quantitatively evaluate the proliferation on seeded mats (n = 3), and cell number was determined using a calibration curve. Cells seeded on tissue culture plates (TCPs) served as the control. Cells seeded on TCPs and treated with 0.5 g of halloysite and kaolin clay were used as controls. At a predetermined time point (24 h), media were removed and the samples were washed with PBS twice to remove unattached cells. Incubation media containing the Alamar Blue was then transferred in a volume of 200 μL to a 96-well plate and fluorescence was measured at 590 nm. To assess cell attachment and proliferation, seeded mats were fixed with 4% paraformaldehyde overnight at 4 °C and observed using a Carl Zeiss Supra field emission scanning electron microscope (Hillsboro, USA—resolution at 1 kV—2.5 nm).

Origin Pro 2018b (Northampton, MA USA) was used to construct the figures containing offset TGA thermograms, derivative TGA thermograms, and XRD patterns. Origin Pro 2018b was also used to generate fiber diameter distribution histograms, BET adsorption–desorption isotherms, BET plots, aPTT assay plots, blood clotting test plots, and cytotoxicity/cell viability assay graphs.

RESULTS AND DISCUSSION

A previously developed wet–wet electrospinning technique[38,39] was employed to produce CNFs and CHNFs in a one-step process. In conventional wet–dry electrospinning, synthetic polymers are generally dissolved in volatile organic solvents, which rapidly evaporate upon the exit of the fiber jet from the needle forming a fiber mat on dry metal collectors.[54] In contrast, in wet–wet electrospinning, a polymer is dissolved in a nonvolatile primary solvent and electrospun into a coagulation bath collector containing a secondary nonsolvent for the polymer. The primary solvent, in which the polymer is dissolved, is miscible with the secondary solvent so that the primary solvent is drawn away from the polymer, resulting in its precipitation in the coagulation bath collector. Thus, in wet–wet electrospinning, fiber formation occurs through precipitation in the coagulation bath not through the solvent evaporation occurring in wet–dry electrospinning.

In this study, cellulose was dissolved in RTIL and electrospun into a water bath. As cellulose coagulates, it forms an intermediate hydrogel with water migrating into the fibers concomitant with RTIL diffusion into the water bath.[55] The hydrogel ultimately collapses into CNFs that are collected and freeze-dried to obtain nonwoven CNF balls. In contrast, simple air-drying results in the collapse of morphology resulting in a cellulose mat. When the coagulation bath containing water is replaced with an aqueous suspension of halloysite nanoclay, the intermediate hydrogel entrains halloysite in the surface of the CNFs and cellulose–halloysite nanofiber balls are collected by freeze-drying (see the Supporting Information Video). This process physically embeds halloysite clay nanoparticles primarily on the surface of the fibers during the intermediate hydrogel state of cellulose in the coagulation bath. The freeze-dried CHNFs appear identical to cotton balls but with an off-white color because of their halloysite surface (Figure 1c).

TGA in Figure 2 shows that the CHNFs left a higher residual mass at 1000 °C when compared to MCHNFs and

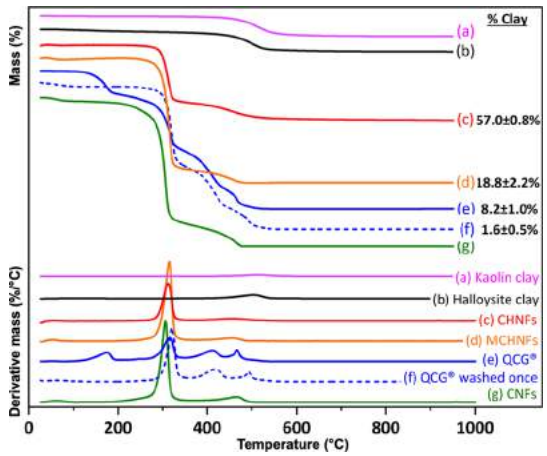

Figure 2. TGA analysis. Amount of clay in the fiber composites studied demonstrated by residual mass at 1000 °C. The residual mass of CHNFs is statistically different from the residual mass of QCG (n = 3, p < 0.001).

QCG. The residual mass corresponds to halloysite nanoclay and the amount of clay present in the CHNFs was calculated to be 57.0 ± 0.8%. In contrast, the MCHNFs contained only 18.8 ± 2.2% halloysite nanoclay, making our one-step fabrication process superior to commercial processes. Similarly, the amount of kaolin clay in QCG based on residual mass was 8.2 ± 1.0%, and this amount was reduced to 1.6 ± 0.5% after a single washing step. Thus, we conclude that CHNFs have approximately 7 times more active clay than QCG.

The major mass loss of neat halloysite and kaolin clay occurred over the temperature range of 400–600 °C, consistent with the dehydroxylation of structural Al–OH groups in the endothermic dehydration of clay.[56] The CNFs showed the two characteristic decompositions associated with combustion and smoldering of cellulose taking place at 200–350 and 400–500 °C, respectively.[38,57] The purity of CNFs was substantiated by the absence of decomposition peaks associated with hemicellulose (~220 °C)[58] and lignin (~100 °C) impurities.[59]

Halloysite nanoclay used to fabricate the CHNF composite appeared to have the typical tubular morphology with diameters ranging from 30 to 120 nm (Figure 3a,b).[11] The SEM images showed the common plate morphology of kaolin

DOI: 10.1021/acsami.9b04615
ACS Appl. Mater. Interfaces 2019, 11, 15447–15456

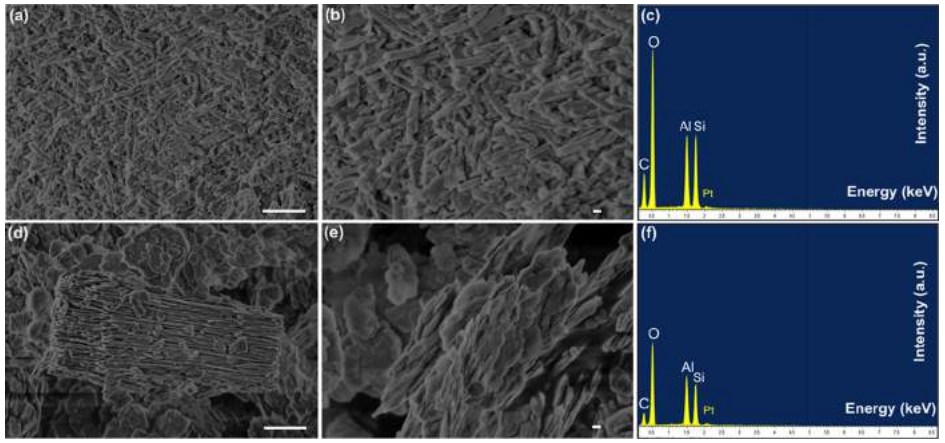

Figure 3. Morphology and elemental composition of the clay samples. SEM images of halloysite nanoclay (a) magnification 50 000× and (b) magnification 100 000×, SEM images of kaolin clay (d) magnification 50 000× and (e) magnification 100 000×, and EDX spectra of (c) halloysite nanoclay and (f) kaolin clay. Scale bar 1 μm (a,d) and 100 nm (b,e).

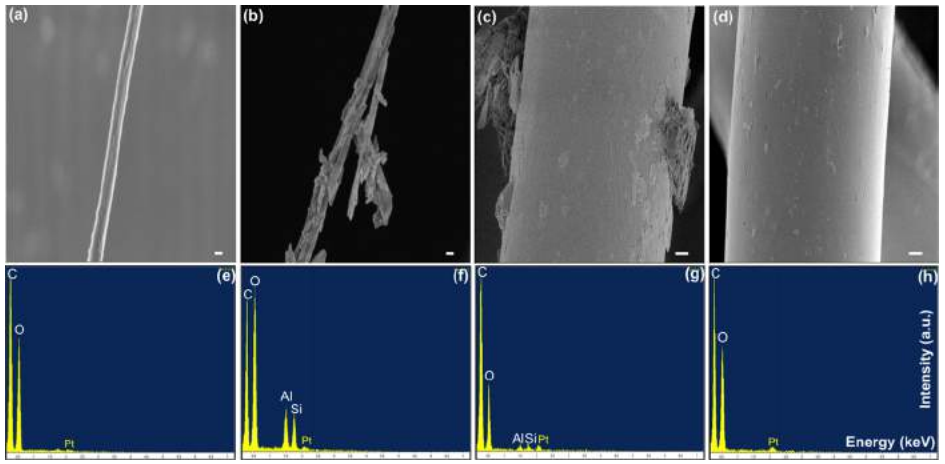

Figure 4. Morphology and elemental composition of the fiber samples. SEM image (a) and EDX spectrum (e) of an electrospun CNF (magnification 100 000×), SEM image (b) and EDX spectrum (f) of an electrospun CHNF washed once (magnification 100 000×), SEM image (c) and EDX spectrum (g) of a microfiber of QCG (magnification 20 000×), and SEM image (d) and EDX spectrum (h) of a microfiber of QCG washed once (magnification 20 000×). Scale bar 100 nm (a,b) and 1 μm (c,d).

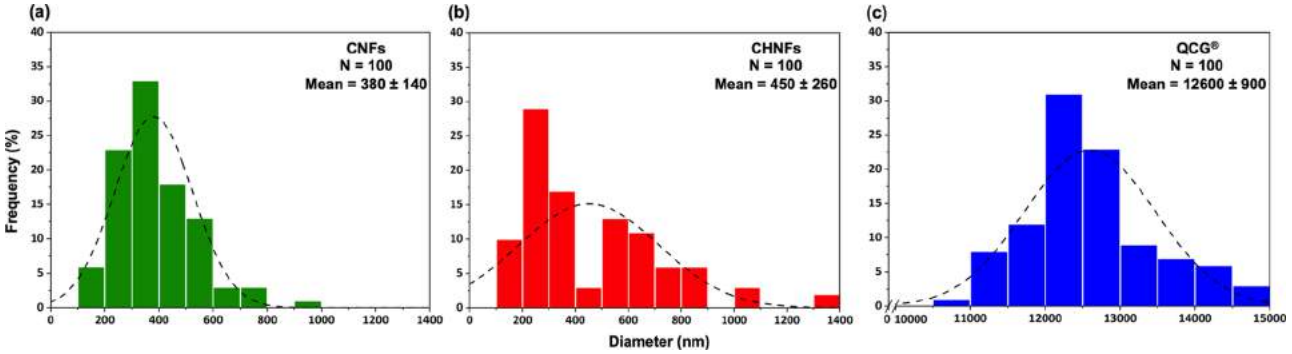

Figure 5. Histograms of the diameter distribution of the fiber samples. Fiber diameter histograms of cellulose (a), CHNFs (b), and QCG combat gauze (c) observed during SEM imaging. The mean diameter of CHNFs and CNFs is statistically different from that of QCG ($p < 0.001$).

clay, the clotting agent used in QCG (Figure 3d,e). In contrast to halloysite nanoclay, kaolin clay flakes stack together to form large agglomerates (Figure 3d).[60] EDX analysis of both clay samples resulted in the same elemental composition as they are chemically identical (Figure 3c,f).[12]

Electrospun CNFs have a cylindrical structure (Figure 4a) with an average diameter of 380 ± 140 nm (Figure 5a). This is consistent with previous studies conducted on electrospun CNFs.[61] The EDX spectrum of cellulose (Figure 4e) reveals the characteristic Kα_1 X-ray peaks corresponding to carbon (0.277 keV) and oxygen (0.525 keV).[39] CHNFs were much smaller in size (see the SEM image in Figure 4b) with an average diameter of 450 ± 260 nm (Figure 5b). In contrast,

DOI: 10.1021/acsami.9b04615
ACS Appl. Mater. Interfaces 2019, 11, 15447−15456

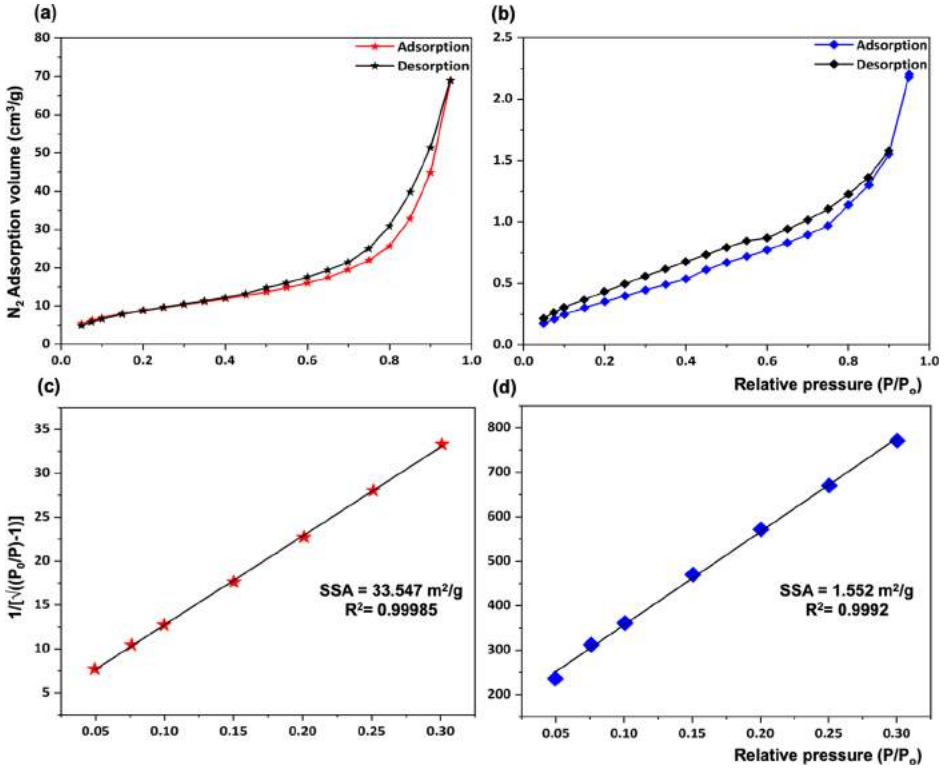

Figure 6. Surface area analysis of the composite fibers. Nitrogen adsorption−desorption isotherms (a,b) and the BET plots/Langmuir fits (c,d) of CHNFs (a,c) and QCG (b,d).

QCG is composed of micron-sized fibers ranging from 11 to 15 μm with an average diameter of 12.6 ± 0.9 μm (Figure 5c).

The surface of CHNFs was completely covered with halloysite nanoclay particles, while QCG showed a sparse kaolin clay coating of the microfiber (Figure 4c). The EDX spectrum of CHNFs (Figure 4f) validated this observation, displaying higher-intensity Kα_1 X-ray peaks for Al (1.487 keV) and Si (1.740 keV) than those observed in the EDX spectrum of QCG (Figure 4g). The loss of significant amounts of kaolin clay after a single water wash was evident in the SEM image of washed QCG (Figure 4d). This observation was confirmed by the absence of the characteristic Al and Si X-ray peaks in the EDX spectrum of washed QCG (Figure 4h). Even though hydrogen is present in all the samples, it cannot be detectable in EDX because of its inability to generate characteristic X-rays. For additional SEM images and EDX spectra of composite fibers, see Figures S1 and S2.

XRD analysis further supported the conclusions made based on TGA, SEM, and EDX studies (Figure S3). The XRD pattern of CHNFs was identical to that of the neat halloysite nanoclay,[16,56,62] and peaks belonging to cellulose[63,64] were not apparent. This verifies the abundance of halloysite nanoclay coating on the surface of the CHNFs. In contrast, the XRD pattern of QCG showed broad peaks belonging to cellulose along with the two most intense peaks originating from the kaolin clay.[60] These two peaks were not observed in the XRD pattern of the washed QCG. This supports the conclusion that most of the kaolin clay on the fibers was lost after a single washing step. Moreover, the crystallinity of both halloysite and kaolin clays was retained in the composite fibers.

The specific surface area of the composite fibers was calculated using BET isotherms (Figure 6). CHNFs showed a significantly higher specific surface area (33.6 m^2 g^{-1}) compared with QCG (1.6 m^2 g^{-1}). This represents nearly 6 times the specific surface area of CNFs (5.7 m^2 g^{-1}). The additional surface area of CHNFs must result from the nanoclay particles coating the fiber surface. The specific surface area of the washed QCG was 3.5 m^2 g^{-1}. This corresponds to approximately 125% increase in the specific surface area of QCG (see Figure S4). This could result from the removal of large flaky agglomerates of kaolin clay from the QCG fibers during the washing step.[65]

The TGA, SEM, EDX, XRD, and BET characterization results all conclusively demonstrate the removal of kaolin clay from QCG even after a single washing step. Thus, in severe bleeding cases or identical wetting in the field, the procoagulant clay particles are rapidly lost, which will result in reduced procoagulant activity for QCG. In contrast, the CHNFs not only show a higher initial clay loading but also remarkably less leaching of halloysite nanoclay particles from the fibers.

The procoagulant activity and stability of the CHNFs were next confirmed by the plasma clotting studies using the aPTT assay. The aPTT assay was used because hemostatic clotting agents affect the coagulation cascade through the intrinsic pathway, which the aPTT clotting assay measures.[3,66,67] Phyllosilicate hemostatic agents such as kaolin, halloysite, and bentonite activate factor XII, which causes coagulation through the intrinsic pathway.[7,68] The presence of tissue factor is needed to activate the extrinsic coagulation pathway, which is not present on the hemostatic agent (and, thus, not present in the aPTT assay).[69] The CHNFs generate the fastest average plasma coagulation time of all samples tested, 143 ± 19 s (Figure 7). This coagulation time is 2.4 times faster than that observed for QCG, 244 ± 41 s. Both CHNFs and QCG

DOI: 10.1021/acsami.9b04615
ACS Appl. Mater. Interfaces 2019, 11, 15447−15456

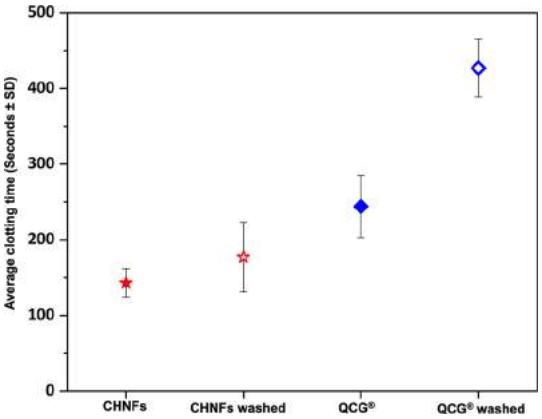

Figure 7. aPTT assay. The time taken to form a fibrin clot in a citrated plasma sample is shown. CHNFs are represented in red stars and QCG in blue diamonds. CHNFs before and after washing are statistically different from QCG before and after washing, respectively (n = 10, p < 0.05).

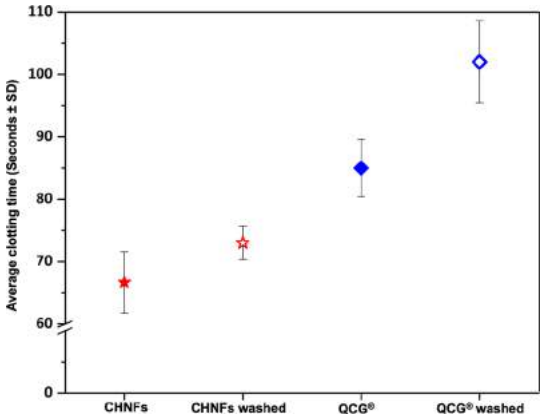

Figure 8. Results of the blood clotting test. The time taken to form a blood clot in a citrated bovine blood sample is shown. CHNFs are represented in red stars and QCG in blue diamonds. CHNFs before and after washing are statistically different from QCG before and after washing, respectively (n = 3, p < 0.01).

performed better than CNFs, which took over 27 min to coagulate the plasma (Figure S5).

It has been shown that there is a correlation between reduction in the aPTT coagulation time (intrinsic pathway) compared to control, even without any reduction in the prothrombin time (extrinsic pathway), with drastically reduced times for the clotting of the femoral artery of rabbits.[3] As the CHNFs reduced the coagulation time of human plasma by 70% compared with the QCG gold standard clotting agent, it is reasonable to conclude that these results should translate into reduced clotting times in animal testing and preclude the need for such testing in proof of concept. Furthermore, QCG has been successfully evaluated in the clotting of porcine blood in vivo.[70] As our CHNFs outperformed the QCG, it is reasonable to conclude that our results would translate into reduced clotting times for pigs as well. CHNFs and QCG both showed reduced procoagulant performance after a single washing step with water, although CHNF clotting performance reduced by only 24% compared to a 75% performance loss for QCG (Figure 7). It is worth noting that the CHNF composite had also been thoroughly washed with both water and ethanol in its preparation to remove the residual ionic liquid. Thus, it is not surprising that the additional washing step of the CHNFs with water resulted in only a slight reduction in the procoagulant activity (Figure 7). An additional advantage of CHNFs is that the average plasma coagulation time of halloysite clay is 55 s faster than kaolin clay, making the halloysite nanoclay superior to kaolin.

The results of the blood clotting test showed the fastest average clotting time for CHNFs, 67 ± 5 s (Figure 8). The QCG sample clotted blood in 85 ± 5 s but lost 20% of its clotting performance after one wash with water compared to 9% performance loss for CHNFs.

hFB cells were grown on fiber mats. An equivalent number of cells for each sample (Figure S6), calculated from reduced Alamar Blue, was determined 24 h after cell seeding. CNFs, CHNFs, and QCG fiber mats showed statistically significant lower metabolic activity than the control TCPs (p < 0.05). Because cellular adhesion is not a favorable outcome when using these blood clotting gauzes, it is thus a positive design characteristic for these composites. When comparing fiber samples, QCG showed statistically insignificant metabolic activity compared with the CHNFs. These results show that the cytotoxicity/cell viability is comparable to the FDA-approved QCG. The compatibility of hFB cells exposed to equal amounts of kaolin clay and halloysite clay was also evaluated. The data showed that both clay samples have reduced metabolic activity compared to the control TCPs. Although the average number of cells proliferated on the halloysite clay was less than that of the kaolin clay, a t-test revealed that the difference between the means was not statistically significant. Another control examined in this study was electrospun CNF mats. This group showed less, although statistically insignificant, metabolic activity than QCG. Even though the cell attachment is less than the control TCPs after 24 h, the SEM images of CHNFs (Figure S7) showed that the attached hFB cells proliferated after 3 days. This confirms that the cells were able to adhere and grow on the CHNFs.

CONCLUSIONS

The halloysite-coated CNFs (CHNFs) clot human plasma and bovine whole blood 2.4 and 1.3 times faster than the commercial QCG, respectively. Two synergistic effects can explain the high performance of the CHNFs. First, the CHNFs had 7 times higher clay loading compared to QCG, 57.0 ± 0.8 and 8.2 ± 1.0%, respectively. This resulted in part by the high surface area of the electrospun CHNFs. The CHNFs had 22 times greater specific surface area compared to QCG, 33.6 and 1.6 $m^2\ g^{-1}$, respectively. The smaller average diameter of the CHNFs (450 ± 260 nm) compared to QCG (12.6 ± 0.9 μm) accounts for part of this increase in surface area. The wet−wet electrospinning process relying on a coagulation bath containing the clay suspension was critical for obtaining high clay loadings, also leading to increased specific surface areas. Fibers electrospun into the clay suspension had 3-fold higher clay loading than when CNFs were simply immersed in a halloysite clay suspension to prepare MCHNFs. The choice of halloysite nanoclay in place of kaolin clay further enhanced the performance. Neat halloysite nanoclay coagulates human plasma approximately 1.6 times faster than neat kaolin clay. Thus, a combination of higher surface area supplied by the electrospun fibers and improved clotting performance of the halloysite nanoclay enhanced the overall plasma clotting performance of the CHNFs. The CHNFs also exhibited

DOI: 10.1021/acsami.9b04615
ACS Appl. Mater. Interfaces 2019, 11, 15447−15456

noncytotoxicity and cell viability with hFB, rendering this composite a safe biocompatible material.

Furthermore, the CHNFs retained over 3 times the human plasma clotting activity compared with the QCG after washing once with water, losing only 24% of its clotting activity compared to a 75% loss of procoagulant activity observed for QCG. The CHNFs also retained more than twice the bovine whole blood clotting activity than QCG. This inherent stability of CHNFs is extremely important for stopping traumatic external hemorrhages on the battlefield and in the operating room as continuous blood flow greatly reduces the performance of QCG. When the QCG was subjected to washing in distilled water, nearly 80% of its clay content was quickly lost. The intermediate hydrogel state formed in the coagulation bath during the wet−wet electrospinning process facilitates kinetic entrapment of halloysite nanoclay particles giving rise to higher clay retention of the CHNFs. This physical embedding of nanoclay particles during the electrospinning process does not occur with simple immersion of prefabricated CNFs in a clay suspension, which is the same process used to produce QCG.

■ ASSOCIATED CONTENT

Supporting Information

The Supporting Information is available free of charge on the ACS Publications website at DOI: 10.1021/acsami.9b04615.

SEM images with EDX spectra, XRD analysis, nitrogen adsorption−desorption isotherms, and the BET plots/Langmuir fits after subjecting to a washing step; aPTT assay results of the controls; cytotoxicity/cell viability assay results; and SEM images showing the cell growth and differentiation of human fibroblast cells cultured on CHNFs (PDF)

Fabrication of cellulose−halloysite nanofibers by electrospinning (AVI)

■ AUTHOR INFORMATION

Corresponding Author

*E-mail: linhar@rpi.edu. Phone: (518) 276-3404.

ORCID

Ranodhi N. Udangawa: 0000-0001-7482-7260

Paiyz Esmat Mikael: 0000-0003-4679-9770

Trevor John Simmons: 0000-0003-4411-8943

Robert J. Linhardt: 0000-0003-2219-5833

Author Contributions

The study was performed by R.N.U., P.E.M, C.M., C.F.W., and C.C., and the manuscript was written by R.N.U. and R.J.L. All authors have given their approval to the final version of this manuscript.

Notes

The authors declare no competing financial interest.

■ ACKNOWLEDGMENTS

The authors duly acknowledge the following people for their assistance in handling characterization instruments: Manager of Energy Materials and Devices Core Facility Collin W. Hitchcock for BET surface area analysis; manager of electron microscopy laboratory Raymond P. Dove for SEM assistance; Senior Application Engineer, Center for Integrated Electronics, M. David Frey for SEM and EDX assistance; and Analytical Core Facility director Dr. Joel Morgan for XRD and TGA assistance. Finally, the authors would like to thank their fellow researchers and colleagues for their support rendered during this project. This work was funded in part by the National Institutes of Health grant no. CA231074.

■ REFERENCES

(1) Pogorielov, M.; Kalinkevich, O.; Deineka, V.; Garbuzova, V.; Solodovnik, A.; Kalinkevich, A.; Kalinichenko, T.; Gapchenko, A.; Sklyar, A.; Danilchenko, S. Haemostatic Chitosan Coated Gauze: In Vitro Interaction with Human Blood and in-Vivo Effectiveness. *Biomater. Res.* **2015**, *19*, 22.

(2) Kozen, B. G.; Kircher, S. J.; Henao, J.; Godinez, F. S.; Johnson, A. S. An Alternative Hemostatic Dressing: Comparison of Celox, Hemcon, and Quikclot. *Acad. Emerg. Med.* **2008**, *15*, 74−81.

(3) Chen, Z.; Li, F.; Liu, C.; Guan, J.; Hu, X.; Du, G.; Yao, X.; Wu, J.; Tian, F. Blood Clot Initiation by Mesoporous Silica Nanoparticles: Dependence on Pore Size or Particle Size? *J. Mater. Chem. B* **2016**, *4*, 7146−7154.

(4) Huey, R. J.; Lo, D.; Burns, D. J.; Basadonna, G.; Hursey, F. X. Clay-Based Hemostatic Agents and Devices for the Delivery Thereof. U.S. Patent 7,968,114 B2, June 28, 2011.

(5) Hardy, C.; Johnson, E. L.; Luksch, P. Hemostatic Material. U.S. Patent 8,106,030 B2, 2012.

(6) Huey, R. J.; Lo, D.; Burns, D. J.; Basadonna, G.; Hursey, F. X. Clay-Based Hemostatic Agents. U.S. Patent 0,228,934 A1, Oct 02, 2018.

(7) Alavi, M.; Totonchi, A.; Okhovat, M. A.; Motazedian, M.; Rezaei, P.; Atefi, M. The Effect of a New Impregnated Gauze Containing Bentonite and Halloysite Minerals on Blood Coagulation and Wound Healing. *Blood Coagul. Fibrinolysis* **2014**, *25*, 856−859.

(8) Lo, D. Hemostatic Fibrous Material. U.S. Patent 0,004,636 A1, Jan 05, 2012.

(9) Ninan, N.; Muthiah, M.; Park, I.-K.; Wong, T. W.; Thomas, S.; Grohens, Y. Natural Polymer/Inorganic Material Based Hybrid Scaffolds for Skin Wound Healing. *Polym. Rev.* **2015**, *55*, 453−490.

(10) Hangge, P.; Stone, J.; Albadawi, H.; Zhang, Y. S.; Khademhosseini, A.; Oklu, R. Hemostasis and Nanotechnology. *Cardiovasc. Diagn. Ther.* **2017**, *7*, S267−S275.

(11) De Silva, R. T.; Dissanayake, R. K.; Mantilaka, M. M. M. G. P. G.; Wijesinghe, W. P. S. L.; Kaleel, S. S.; Premachandra, T. N.; Weerasinghe, L.; Amaratunga, G. A. J.; De Silva, K. M. N. Drug-Loaded Halloysite Nanotube-Reinforced Electrospun Alginate-Based Nanofibrous Scaffolds with Sustained Antimicrobial Protection. *ACS Appl. Mater. Interfaces* **2018**, *10*, 33913−33922.

(12) Levis, S. R.; Deasy, P. B. Characterisation of Halloysite for Use as a Microtubular Drug Delivery System. *Int. J. Pharm.* **2002**, *243*, 125−134.

(13) Massaro, M.; Lazzara, G.; Milioto, S.; Noto, R.; Riela, S. Covalently Modified Halloysite Clay Nanotubes: Synthesis, Properties, Biological and Medical Applications. *J. Mater. Chem. B* **2017**, *5*, 2867−2882.

(14) Vergaro, V.; Abdullayev, E.; Lvov, Y. M.; Zeitoun, A.; Cingolani, R.; Rinaldi, R.; Leporatti, S. Cytocompatibility and Uptake of Halloysite Clay Nanotubes. *Biomacromolecules* **2010**, *11*, 820−826.

(15) Liu, H.-Y.; Du, L.; Zhao, Y.-T.; Tian, W.-Q. In Vitro Hemocompatibility and Cytotoxicity Evaluation of Halloysite Nanotubes for Biomedical Application. *J. Nanomater.* **2015**, *2015*, 685323.

(16) Lun, H.; Ouyang, J.; Yang, H. Natural Halloysite Nanotubes Modified as an Aspirin Carrier. *RSC Adv.* **2014**, *4*, 44197−44202.

(17) Xue, J.; Niu, Y.; Gong, M.; Shi, R.; Chen, D.; Zhang, L.; Lvov, Y. Electrospun Microfiber Membranes Embedded with Drug-Loaded Clay Nanotubes for Sustained Antimicrobial Protection. *ACS Nano* **2015**, *9*, 1600−1612.

(18) Swatloski, R. P.; Spear, S. K.; Holbrey, J. D.; Rogers, R. D. Dissolution of Cellulose with Ionic Liquids. *J. Am. Chem. Soc.* **2002**, *124*, 4974−4975.

DOI: 10.1021/acsami.9b04615
ACS Appl. Mater. Interfaces 2019, 11, 15447−15456

(19) Rodríguez, K.; Gatenholm, P.; Renneckar, S. Electrospinning Cellulosic Nanofibers for Biomedical Applications: Structure and in Vitro Biocompatibility. *Cellulose* **2012**, *19*, 1583−1598.
(20) Cooley, J. F. Apparatus for Electrically Dispersing Fluids. U.S. Patent 692,631 A, Feb 04, 1902.
(21) Chen, Z. G.; Wang, P. W.; Wei, B.; Mo, X. M.; Cui, F. Z. Electrospun Collagen−Chitosan Nanofiber: A Biomimetic Extracellular Matrix for Endothelial Cell and Smooth Muscle Cell. *Acta Biomater.* **2010**, *6*, 372−382.
(22) Lalia, B. S.; Guillen-Burrieza, E.; Arafat, H. A.; Hashaikeh, R. Fabrication and Characterization of Polyvinylidenefluoride-Co-Hexafluoropropylene (Pvdf-Hfp) Electrospun Membranes for Direct Contact Membrane Distillation. *J. Membr. Sci.* **2013**, *428*, 104−115.
(23) Teo, W. E.; Ramakrishna, S. A Review on Electrospinning Design and Nanofibre Assemblies. *Nanotechnology* **2006**, *17*, R89.
(24) Medronho, B.; Romano, A.; Miguel, M. G.; Stigsson, L.; Lindman, B. Rationalizing Cellulose (in) Solubility: Reviewing Basic Physicochemical Aspects and Role of Hydrophobic Interactions. *Cellulose* **2012**, *19*, 581−587.
(25) Quan, S.-L.; Kang, S.-G.; Chin, I.-J. Characterization of Cellulose Fibers Electrospun Using Ionic Liquid. *Cellulose* **2010**, *17*, 223−230.
(26) Freire, M. G.; Teles, A. R. R.; Ferreira, R. A. S.; Carlos, L. D.; Lopes-da-Silva, J. A.; Coutinho, J. A. P. Electrospun Nanosized Cellulose Fibers Using Ionic Liquids at Room Temperature. *Green Chem.* **2011**, *13*, 3173−3180.
(27) Isik, M.; Sardon, H.; Mecerreyes, D. Ionic Liquids and Cellulose: Dissolution, Chemical Modification and Preparation of New Cellulosic Materials. *Int. J. Mol. Sci.* **2014**, *15*, 11922−11940.
(28) Xu, S.; Zhang, J.; He, A.; Li, J.; Zhang, H.; Han, C. C. Electrospinning of Native Cellulose from Nonvolatile Solvent System. *Polymer* **2008**, *49*, 2911−2917.
(29) Frey, M. W. Electrospinning Cellulose and Cellulose Derivatives. *Polym. Rev.* **2008**, *48*, 378−391.
(30) Kim, C.-W.; Kim, D.-S.; Kang, S.-Y.; Marquez, M.; Joo, Y. L. Structural Studies of Electrospun Cellulose Nanofibers. *Polymer* **2006**, *47*, 5097−5107.
(31) Quan, S.-L.; Kang, S.-G.; Chin, I.-J. Characterization of Cellulose Fibers Electrospun Using Ionic Liquid. *Cellulose* **2010**, *17*, 223−230.
(32) Mahadeva, S. K.; Kim, J. Influence of Residual Ionic Liquid on the Thermal Stability and Electromechanical Behavior of Cellulose Regenerated from 1-Ethyl-3-Methylimidazolium Acetate. *Fibers Polym.* **2012**, *13*, 289−294.
(33) Huey, R.; Lo, D.; Burns, D. J. Clay-Based Hemostatic Agents and Devices for the Delivery Thereof. U.S. Patent 7,604,819 B2, Oct 20, 2009.
(34) Arnaud, F.; Tomori, T.; Carr, W.; McKeague, A.; Teranishi, K.; Prusaczyk, K.; McCarron, R. Exothermic Reaction in Zeolite Hemostatic Dressings: QuikClot ACS and ACS+. *Ann. Biomed. Eng.* **2008**, *36*, 1708.
(35) Sena, M. J.; Douglas, G.; Gerlach, T.; Grayson, J. K.; Pichakron, K. O.; Zierold, D. A Pilot Study of the Use of Kaolin-Impregnated Gauze (Combat Gauze) for Packing High-Grade Hepatic Injuries in a Hypothermic Coagulopathic Swine Model. *J. Surg. Res.* **2013**, *183*, 704−709.
(36) Kelly, J. F.; Ritenour, A. E.; McLaughlin, D. F.; Bagg, K. A.; Apodaca, A. N.; Mallak, C. T.; Pearse, L.; Lawnick, M. M.; Champion, H. R.; Wade, C. E. Injury Severity and Causes of Death from Operation Iraqi Freedom and Operation Enduring Freedom: 2003−2004 Versus 2006. *J. Trauma: Inj., Infect., Crit. Care* **2008**, *64*, S21−S27.
(37) Liu, X.; Lin, T.; Gao, Y.; Xu, Z.; Huang, C.; Yao, G.; Jiang, L.; Tang, Y.; Wang, X. Antimicrobial Electrospun Nanofibers of Cellulose Acetate and Polyester Urethane Composite for Wound Dressing. *J. Biomed. Mater. Res., Part B* **2012**, *100B*, 1556−1565.
(38) Zheng, Y.; Miao, J.; Maeda, N.; Frey, D.; Linhardt, R. J.; Simmons, T. J. Uniform Nanoparticle Coating of Cellulose Fibers During Wet Electrospinning. *J. Mater. Chem. A* **2014**, *2*, 15029−15034.
(39) Hou, L.; Udangawa, W. M. R. N.; Pochiraju, A.; Dong, W.; Zheng, Y.; Linhardt, R. J.; Simmons, T. J. Synthesis of Heparin-Immobilized, Magnetically Addressable Cellulose Nanofibers for Biomedical Applications. *ACS Biomater. Sci. Eng.* **2016**, *2*, 1905−1913.
(40) Miyauchi, M.; Miao, J.; Simmons, T. J.; Lee, J.-W.; Doherty, T. V.; Dordick, J. S.; Linhardt, R. J. Conductive Cable Fibers with Insulating Surface Prepared by Coaxial Electrospinning of Multiwalled Nanotubes and Cellulose. *Biomacromolecules* **2010**, *11*, 2440−2445.
(41) Miyauchi, M.; Miao, J.; Simmons, T.; Dordick, J.; Linhardt, R. Flexible Electrospun Cellulose Fibers as an Affinity Packing Material for the Separation of Bovine Serum Albumin. *J. Chromatogr. Sep. Tech.* **2011**, *2*, 110.
(42) Miao, J.; Pangule, R. C.; Paskaleva, E. E.; Hwang, E. E.; Kane, R. S.; Linhardt, R. J.; Dordick, J. S. Lysostaphin-Functionalized Cellulose Fibers with Antistaphylococcal Activity for Wound Healing Applications. *Biomaterials* **2011**, *32*, 9557−9567.
(43) Liu, H.; Hsieh, Y.-L. Ultrafine Fibrous Cellulose Membranes from Electrospinning of Cellulose Acetate. *J. Polym. Sci., Part B: Polym. Phys.* **2002**, *40*, 2119−2129.
(44) Zheng, Y.; Cai, C.; Zhang, F.; Monty, J.; Linhardt, R. J.; Simmons, T. J. Can Natural Fibers Be a Silver Bullet? Antibacterial Cellulose Fibers through the Covalent Bonding of Silver Nanoparticles to Electrospun Fibers. *Nanotechnology* **2016**, *27*, 055102.
(45) Vatankhah, E.; Semnani, D.; Prabhakaran, M. P.; Tadayon, M.; Razavi, S.; Ramakrishna, S. Artificial Neural Network for Modeling the Elastic Modulus of Electrospun Polycaprolactone/Gelatin Scaffolds. *Acta Biomater.* **2014**, *10*, 709−721.
(46) Mahadeva, S. K.; Kim, J. Influence of Residual Ionic Liquid on the Thermal Stability and Electromechanical Behavior of Cellulose Regenerated from 1-Ethyl-3-Methylimidazolium Acetate. *Fibers Polym.* **2012**, *13*, 289−294.
(47) Blaine, R. L.; Rose, J. E. Validation of Thermogravimetric Analysis Performance Using Mass Loss Reference Materials. TA Instruments [Online] 2009, p 1−10. http://www.tainstruments.com/pdf/literature/TA316a.pdf (accessed Oct 01, 2018).
(48) Liu, S.; Yan, Q.; Tao, D.; Yu, T.; Liu, X. Highly Flexible Magnetic Composite Aerogels Prepared by Using Cellulose Nanofibril Networks as Templates. *Carbohydr. Polym.* **2012**, *89*, 551−557.
(49) Kretz, C.; Cuddy, K.; Stafford, A.; Fredenburgh, J.; Roberts, R.; Weitz, J. HD1, a thrombin- and prothrombin-binding DNA aptamer, inhibits thrombin generation by attenuating prothrombin activation and thrombin feedback reactions. *Thromb. Haemostasis* **2010**, *103*, 83−96.
(50) Weiner, M. Residual Serum Thrombin Activity. *Clin. Chem.* **1958**, *4*, 271−277.
(51) Zolfagharian, H.; Mohajeri, M.; Babaie, M. Honey Bee Venom (Apis Mellifera) Contains Anticoagulation Factors and Increases the Blood-Clotting Time. *J. Pharmacopuncture* **2015**, *18*, 7.
(52) Osoniyi, O.; Onajobi, F. Coagulant and Anticoagulant Activities in Jatropha Curcas Latex. *J. Ethnopharmacol.* **2003**, *89*, 101−105.
(53) Pawlaczyk, I.; Czerchawski, L.; Kańska, J.; Bijak, J.; Capek, P.; Pliszczak-Król, A.; Gancarz, R. An Acidic Glycoconjugate from Lythrum Salicaria L. With Controversial Effects on Haemostasis. *J. Ethnopharmacol.* **2010**, *131*, 63−69.
(54) Carvalho, M. S.; Silva, J. C.; Udangawa, R. N.; Cabral, J. M. S.; Ferreira, F. C.; da Silva, C. L.; Linhardt, R. J.; Vashishth, D. Co-Culture Cell-Derived Extracellular Matrix Loaded Electrospun Microfibrous Scaffolds for Bone Tissue Engineering. *Mater. Sci. Eng., C* **2019**, *99*, 479−490.
(55) Udangawa, W. M. R. N.; Willard, C. F.; Mancinelli, C.; Chapman, C.; Linhardt, R. J.; Simmons, T. J. Coconut Oil-Cellulose Beaded Microfibers by Coaxial Electrospinning: An Eco-Model System to Study Thermoregulation of Confined Phase Change Materials. *Cellulose* **2019**, *26*, 1855−1868.
(56) Sun, P.; Liu, G.; Lv, D.; Dong, X.; Wu, J.; Wang, D. Effective Activation of Halloysite Nanotubes by Piranha Solution for Amine

DOI: 10.1021/acsami.9b04615
ACS Appl. Mater. Interfaces 2019, 11, 15447−15456

Modification Via Silane Coupling Chemistry. *RSC Adv.* **2015**, *5*, 52916−52925.
(57) Antal, M. J. J.; Varhegyi, G. Cellulose Pyrolysis Kinetics: The Current State of Knowledge. *Ind. Eng. Chem. Res.* **1995**, *34*, 703−717.
(58) Werner, K.; Pommer, L.; Broström, M. Thermal Decomposition of Hemicelluloses. *J. Anal. Appl. Pyrolysis* **2014**, *110*, 130−137.
(59) Watkins, D.; Nuruddin, M.; Hosur, M.; Tcherbi-Narteh, A.; Jeelani, S. Extraction and Characterization of Lignin from Different Biomass Resources. *J. Mater. Res. Technol.* **2015**, *4*, 26−32.
(60) Chen, C. Y.; Lan, G. S.; Tuan, W. H. Microstructural Evolution of Mullite During the Sintering of Kaolin Powder Compacts. *Ceram. Int.* **2000**, *26*, 715−720.
(61) Kim, C.-W.; Kim, D.-S.; Kang, S.-Y.; Marquez, M.; Joo, Y. L. Structural Studies of Electrospun Cellulose Nanofibers. *Polymer* **2006**, *47*, 5097−5107.
(62) Yuan, P.; Southon, P. D.; Liu, Z.; Green, M. E. R.; Hook, J. M.; Antill, S. J.; Kepert, C. J. Functionalization of Halloysite Clay Nanotubes by Grafting with Γ-Aminopropyltriethoxysilane. *J. Phys. Chem. C* **2008**, *112*, 15742−15751.
(63) Poletto, M.; Pistor, V.; Zattera, A. J. Structural Characteristics and Thermal Properties of Native Cellulose. In *Cellulose-Fundamental Aspects*; Ven, T. G. M. V. D., Godbout, L., Eds.; InTech: London, U.K., 2013; Chapter 2, pp 45−65.
(64) Czaja, W.; Romanovicz, D.; Brown, R. m. Structural Investigations of Microbial Cellulose Produced in Stationary and Agitated Culture. *Cellulose* **2004**, *11*, 403−411.
(65) Siriwardane, I. W.; Udangawa, R.; de Silva, R. M.; Kumarasinghe, A. R.; Acres, R. G.; Hettiarachchi, A.; Amaratunga, G. A. J.; de Silva, K. M. N. Synthesis and Characterization of Nano Magnesium Oxide Impregnated Granular Activated Carbon Composite for H2s Removal Applications. *Mater. Des.* **2017**, *136*, 127−136.
(66) Bates, S. M.; Weitz, J. I. Coagulation Assays. *Circulation* **2005**, *112*, e53−e60.
(67) Francis, J. L.; Groce, J. B., III; Consensus Group, T. H. Challenges in Variation and Responsiveness of Unfractionated Heparin. *Pharmacotherapy* **2004**, *24*, 108S−119S.
(68) Kudela, D.; Smith, S. A.; May-Masnou, A.; Braun, G. B.; Pallaoro, A.; Nguyen, C. K.; Chuong, T. T.; Nownes, S.; Allen, R.; Parker, N. R.; Rashidi, H. H.; Morrissey, J. H.; Stucky, G. D. Clotting Activity of Polyphosphate-Functionalized Silica Nanoparticles. *Angew. Chem., Int. Ed.* **2015**, *54*, 4018−4022.
(69) Mackman, N. The Role of Tissue Factor and Factor Viia in Hemostasis. *Anesth. Analg.* **2009**, *108*, 1447.
(70) Gegel, B.; Burgert, J.; Gasko, J.; Campbell, C.; Martens, M.; Keck, J.; Reynolds, H.; Loughren, M.; Johnson, D. The Effects of Quikclot Combat Gauze and Movement on Hemorrhage Control in a Porcine Model. *Mil. Med.* **2012**, *177*, 1543−1547.

DOI: 10.1021/acsami.9b04615
ACS Appl. Mater. Interfaces 2019, 11, 15447−15456